Energy & Environmental Science

Cite this: *Energy Environ. Sci.*, 2011, **4**, 1311

www.rsc.org/ees

PAPER

820 mV open-circuit voltages from Cu_2O/CH_3CN junctions†

Chengxiang Xiang, Gregory M. Kimball, Ronald L. Grimm, Bruce S. Brunschwig, Harry A. Atwater* and Nathan S. Lewis*

Received 12th October 2010, Accepted 25th November 2010
DOI: 10.1039/c0ee00554a

P-Type cuprous oxide (Cu_2O) photoelectrodes prepared by the thermal oxidation of Cu foils exhibited open-circuit voltages in excess of 800 mV in nonaqueous regenerative photoelectrochemical cells. In contact with the decamethylcobaltocene$^{+/0}$ ($Me_{10}CoCp_2^{+/0}$) redox couple, cuprous oxide yielded open-circuit voltage, V_{oc}, values of 820 mV and short-circuit current density, J_{sc}, values of 3.1 mA cm^{-2} under simulated air mass 1.5 illumination. The energy-conversion efficiency of 1.5% was limited by solution absorption and optical reflection losses that reduced the short-circuit photocurrent density. Spectral response measurements demonstrated that the internal quantum yield approached unity in the 400–500 nm spectral range, but poor red response, attributable to bulk recombination, lowered the overall efficiency of the cell. X-Ray photoelectron spectroscopy and Auger electron spectroscopy indicated that the photoelectrodes had a high-quality cuprous oxide surface, and revealed no observable photocorrosion during operation in the nonaqueous electrolyte. The semiconductor/liquid junctions thus provide a noninvasive method to investigate the energy-conversion properties of cuprous oxide without the confounding factors of deleterious surface reactions.

I. Introduction

Cuprous oxide (Cu_2O) is an attractive material for water photoelectrolysis and for photovoltaics because of the low cost, high availability,[1] and straightforward processing of Cu_2O.[2–4] Cu_2O is a native p-type semiconductor, with a 2.0 eV band gap and a relatively high absorption coefficient in the visible region.[2,3,5,6] Cu_2O synthesized by high temperature thermal oxidation of Cu has been shown to have high hole mobilities and long minority-carrier diffusion lengths.[2,7,8]

The efficiency of Cu_2O solar cells is however limited by the difficulty of preparing high-quality n-type Cu_2O and by the lack of a suitable n-type heterojunction partner. Interfacial chemical reactions at Cu_2O/metal Schottky junctions result in the precipitation of deleterious Cu metal that lowers the barrier height of the resulting Schottky junctions and limits the open-circuit voltage to <350 mV.[2,9] Interfacial Cu formation also degrades the performance of p-Cu_2O heterojunctions[10] formed from metal–insulator–Cu_2O contacts[11] and transparent conducting oxide (TCO)/Cu_2O heterojunctions that incorporate

Beckman Institute and Kavli Nanoscience Institute, Division of Chemistry and Chemical Engineering, 210 Noyes Laboratory, MC 127-72, California Institute of Technology, Pasadena, California, 9125. E-mail: haa@caltech.edu; nslewis@caltech.edu

† Electronic supplementary information (ESI) available: Refractive index and absorption coefficient of Cu_2O substrates (Fig. 1S) and the absorbance spectra for CH_3CN–$Me_{10}CoCp_2^{+/0}$ solution (Fig. 2S) in the spectra range of interest. See DOI: 10.1039/c0ee00554a

Broader context

Low cost, earth-abundant light absorbers are of great interest for use in terrestrial photovoltaics and in artificial photosynthesis. After early research work in the 1980s, cuprous oxide (Cu_2O) has recently received renewed interest for such applications. With a band gap of 2.0 eV, the theoretical efficiency of a Cu_2O-based solar conversion device under AM 1.5 illumination is on the order of 20%. However, the highest efficiency reported to date is 2%, in a p–n heterojunction structure. The major challenge for formation of a highly efficient Cu_2O solid-state cell is the lack of emitter materials that possess suitable band-edge alignment and that do not participate in deleterious interfacial reactions with the cuprous oxide. Semiconductor/liquid junctions offer the opportunity to explore the limits on the open-circuit voltage, V_{oc}, that can be obtained by the use of redox species that have very negative Nernstian redox potentials. In this work, high-quality Cu_2O substrates were produced by high-temperature oxidation of copper foils. P-Type Cu_2O photoelectrodes in contact with the decamethylcobaltocene$^{+/0}$ redox couple displayed V_{oc} values in excess of 800 mV, and near-unity internal quantum yields in the 400–500 nm spectral range.

ZnO, In_2O_3, SnO_2, or CdO.[12–16] Devices with higher barrier heights have been fabricated by minimizing interfacial Cu formation. For example, a Cu_2O/ZnO heterojunction solar cell has been reported to display an open-circuit voltage of 595 mV and an energy-conversion efficiency of 2%.[13]

Semiconductor/liquid junctions present an alternative to conventional solid-state photovoltaic devices. Semiconductor/liquid junctions offer the opportunity to tune the electrical and chemical properties of the interface to produce either highly rectifying or ohmic contacts to a semiconductor of interest.[17–20] In aqueous solutions, cuprous oxide is only thermodynamically stable in a limited range of pH and electrochemical potential.[21] However, in acetonitrile[22] and other nonaqueous electrolytes,[23–25] cuprous oxide exhibits minimal photocorrosion.

The very low energy (3.2 eV *vs.* vacuum)[26] of the conduction-band edge of Cu_2O poses special challenges in forming high barrier-height contacts to this semiconductor. Typically only very reactive metals would be expected to yield high barrier heights in p-Cu_2O/metal Schottky barriers, and these metals would only be useful if thermodynamically allowed interfacial chemical reactions, that produce species such as Cu metal, can be avoided during contact formation. Few heterojunction contacts have the needed low electron affinity to provide suitable band-edge offsets for junctions with Cu_2O. For example, the built-in voltage in Cu_2O/ZnO heterojunctions is only 0.75–0.87 V, due to the band-edge misalignment.[27] High quality p–n Cu_2O homojunctions have not been reported due to the difficulty of preparing n-type Cu_2O. For semiconductor/liquid contacts, redox species that have very negative Nernstian redox potentials should be required theoretically to produce p-Cu_2O/liquid junctions that provide high open-circuit photovoltages and thus high solar energy-conversion efficiencies. The potentials of such species are far more negative than the reduction potential of water to produce H_2, and thus such redox species should be short-lived in aqueous solution. However, the use of one-electron, outer-sphere redox couples that have very negative reduction potentials, such as cobaltocenium/cobaltocene ($CoCp_2^{+/0}$) or decamethylcobaltocenium/decamethylcobaltocene ($Me_{10}CoCp_2^{+/0}$) in inert, nonaqueous solvents offers an opportunity to explore the limits on open-circuit voltage that can be obtained by use of very high barrier height contacts to Cu_2O photocathodes. The performance of such systems, investigated herein, can be used to establish the photovoltage and energy-conversion properties of Cu_2O contacts that do not suffer from interfacial chemical reactions or interdiffusion processes that are typically present in Cu_2O-based solid-state devices.

II. Experimental

A. Preparation of Cu_2O substrates

Large-grain polycrystalline Cu_2O substrates, ~350 μm in thickness, were prepared by the thermal oxidation of 250 μm thick copper sheet (99.9999% pure, Alfa Aesar) that was diced into 6 mm × 6 mm squares. The Cu samples were then suspended in a quartz tube and loaded into a tube furnace. Oxidation to Cu_2O was initiated by heating the tube furnace to 800 °C under $<5 \times 10^{-6}$ Torr. The temperature was ramped to 980 °C under a rough vacuum of 1×10^{-3} Torr and the Cu foil was then oxidized by exposure to oxygen (ultra-high purity, Air Liquide) at 6 Torr for 2 h. Following oxidation, the tube furnace was cooled stepwise to room temperature, under successively decreasing oxygen pressures, to maintain the Cu_2O phase according to the Cu–O phase diagram.[28] The as-oxidized Cu_2O foils were lapped using diamond abrasive films, and polished in a colloidal silica slurry (South Bay Technology), to produce substrates that had a specular finish and a thickness of 100 μm–150 μm, as measured by digital calipers.

B. Characterization of Cu_2O substrates

Scanning electron microscope (SEM) images as well as maps of the crystallographic orientation by Electron Back Scattering Diffraction (EBSD) were collected using a ZEISS 1550. X-Ray diffraction (XRD) data were collected using a Philips XRD with Cu Kα radiation. Square Cu_2O substrates with evaporated gold contacts patterned at the four corners through a shadow mask were used for room temperature Van der Pauw and Hall effect measurements (MMR Technologies).

Spectroscopic ellipsometry was performed at an angle of incidence of 50°, 60°, or 70°, for 300 nm < λ < 850 nm, using a Xe lamp as the light source. The dielectric property $\psi(\omega),\Delta(\omega)$ data were converted to $n(\omega),k(\omega)$ values assuming a bulk, isotropic substrate. The solution absorption of diluted electrolyte in sealed quartz cuvettes was measured using a UV-vis spectrometer (Cary 50).

X-Ray photoelectron spectroscopy (XPS) and X-ray excited Auger electron spectroscopy (XAES, or AES) data were obtained at base pressures $<1 \times 10^{-9}$ Torr using an M-Probe spectrometer. A monochromatic Al Kα source generated X-rays incident on the sample with a 300 μm spot. High-resolution spectra were acquired with a 100 mm hemispherical electron analyzer set to a 20 eV pass energy and controlled using the ESCA 2000 E Capture software (Service Physics). All XP and XAE spectra were energy corrected assuming an adventitious C(1s) photoelectron binding energy peak of 284.6 eV, and fit using a Shirley baseline. The Cu_2O samples were freshly prepared and immediately loaded into the spectrometer. In addition to freshly prepared Cu_2O samples, XP and Auger spectra were also acquired on Cu_2O substrates that had been used as electrodes in photoelectrochemical cells. All Auger and XP spectra were fit using a software package that was written in-house that minimizes the χ^2 fitting error with the Levenberg–Marquardt algorithm. In all cases, spectra were fit with Gaussian–Lorentzian lineshapes above a Shirley background with no asymmetric profiles. The Cu($2p_{3/2}$) XP spectra were well fit with two peaks, with no *a priori* constraints placed on the peak locations, areas, or widths. Conversely, fits to the Cu LMM Auger spectra required up to four peaks. This somewhat more flat optimization space required successive iterations in which the full width at half maximum (FWHM) of the peaks was constrained to 3.0 eV while the peak position was optimized, and the resulting peak positions then were fixed while the peak width was optimized.

C. Photoelectrochemistry and spectral response properties

Cuprous oxide semiconductor electrodes were prepared according to established techniques.[17,29,30] Ohmic contacts were made

by evaporation of 100 nm of gold onto the unpolished side of the Cu_2O substrate. The Cu_2O substrates were then attached to copper wire by use of conductive silver paste between the wire and the gold film on the back of the Cu_2O. Exposed copper, silver, and gold surfaces were sealed to a supporting glass tube using epoxy (Hysol 1C), such that only the polished Cu_2O face was exposed to the electrolyte solution. The front surface of the photoelectrode was etched in 8 M HNO_3 (aq) for 1–2 s, followed by copious rinsing with 18 MΩ resistivity H_2O (Nanopure Infinity, Barnstead), followed by drying in a stream of N_2(g).[12,13]

For all nonaqueous photoelectrochemical experiments, CH_3CN (anhydrous, 99.8%, Sigma Aldrich) was distilled under N_2(g) (ultra-high purity, Air Liquide) from CaH_2 (≥97%, Fluka), $LiClO_4$ (battery grade, 99.99%, Sigma Aldrich) was dried by fusion at 350 °C under $<1 \times 10^{-3}$ Torr and was stored in a VAC Omni-Lab glovebox that had <0.2 ppm of O_2(g). Bis(cyclopentadienyl) cobalt(II) (cobaltocene, $CoCp_2^0$) and bis(pentamethylcyclopentadienyl) cobalt(II) (decamethylcobaltocene, $Me_{10}CoCp_2^0$) were purchased from Sigma Aldrich and were purified by sublimation. Bis(cyclopentadienyl) cobalt(III) hexafluorophosphate (cobaltocenium, $CoCp_2^+ \cdot PF_6^-$) and bis(pentamethylcyclopentadienyl) cobalt(III) hexafluorophosphate (decamethylcobaltocenium, $Me_{10}CoCp_2^+ \cdot PF_6^-$) were purchased from Sigma Aldrich and recrystallized before use.

Current density *vs.* potential (*J*–*E*) data were collected at 50 mV s^{-1} using a Princeton Applied Research (PAR 273) potentiostat. White light from a Sylvania ELH-type halogen bulb was passed through a quartz diffuser to provide the equivalent of air mass 1.5 illumination calibrated using a Si photodiode electrode inside the cell. Various illumination intensities were obtained by use of a combination of quartz neutral density filters. Conventional three-electrode photoelectrochemical cells were assembled in an inert atmosphere glovebox, and included a Pt gauze counter electrode and a Pt wire reference electrode poised at the solution potential. An additional Pt disk working electrode was used to measure the uncompensated ohmic resistance of the cell, typically ~50 Ω. The stir bar was placed directly next to the Cu_2O photoelectrode and was rotated at ~3000 rpm to minimize mass-transport effects. The electrochemical data were analyzed and reported as-collected, without correction for any solution resistance or concentration overpotential losses.[31] Previous work has shown that such three-electrode potentiostatic measurements yield photoelectrode performance characteristics that are very close to, and essentially identical to, those obtained in optimized, unstirred, two-electrode, thin-layer, regenerative, full photoelectrochemical solar cell devices.[30]

Aqueous photoelectrochemical experiments were performed in ~20 mL of 0.5 M K_2SO_4–0.050 M methyl viologen dichloride (MV^{2+}, 98%, Aldrich) that was buffered at pH = 3.6 by potassium hydrogen phthalate. The Nernstian potential of the solution was driven to −0.6 V *vs.* SCE using the large carbon cloth electrode as a working electrode and the frit-separated Pt mesh as a counter electrode. During experiments with the Cu_2O working electrodes, the carbon cloth electrode served as the counter electrode, a Pt wire that was poised at the solution potential served as the reference electrode. The cell was purged with Ar gas at all times, to minimize reaction between O_2(g) and $MV^{+\bullet}$.

Spectral response measurements were performed on a photoelectrochemical cell that contained CH_3CN–1.0 M $LiClO_4$–0.0020 M $Me_{10}CoCp_2^+$–0.0002 M $Me_{10}CoCp_2^0$. Relative to the solution used to collect *J*–*E* data, the solution used for spectral response measurements was diluted with CH_3CN to minimize solution absorption. A 50 W xenon arc lamp (Oriel) was chopped at 13 Hz and passed through a quarter-wave monochromator onto the working electrode in the photoelectrochemical cell. The light intensity was determined using a calibrated Si photodiode that was placed at the same position as the working electrode. A Gamry Reference 600 potentiostat was used to measure the photocurrent at short circuit. Lock-in amplifiers (EG&G Princeton Applied Research) collected signals from both the reference Si photodiode channel and from the potentiostat output channel. The signal from both lock-in amplifiers was fed into a computer that was controlled by a LabVIEW program.

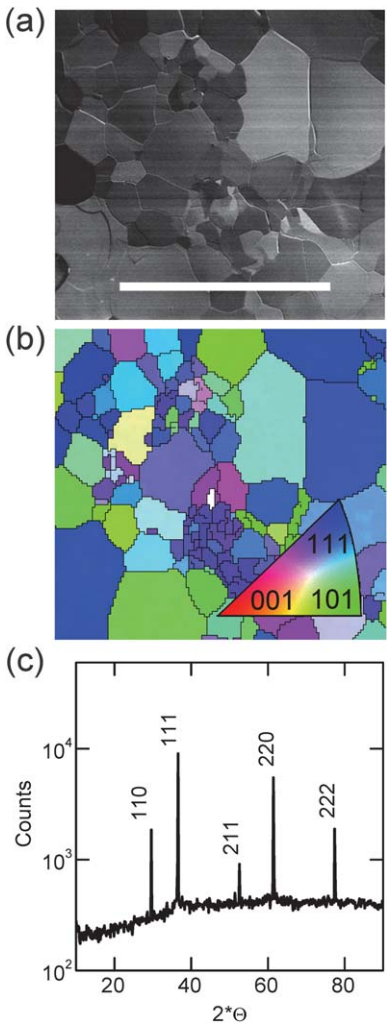

Fig. 1 (a) Scanning electron microscope image showing the polycrystalline grain structure of the Cu_2O foil before lapping and polishing (scale bar, 1 mm). (b) Electron backscatter diffraction image showing the orientation map corresponding to the grain structure of the Cu_2O substrate. (c) X-Ray diffraction measurement showing phase-pure Cu_2O.

III. Results

A. Crystal structure and electrical properties of Cu_2O electrodes

The average grain size of an as-grown Cu_2O substrate was 275 ± 120 μm in diameter, as shown by SEM images (Fig. 1a). Across large sample areas, no strong preferential crystallographic orientation was observed in the substrate, as shown by the corresponding false-color representation of the crystal planes acquired by electron backscatter diffraction (EBSD) (Fig. 1b). The X-ray diffraction pattern of the Cu_2O substrate exhibited reflection peaks that could all be indexed to the Cu_2O cubic structure (Fig. 1c). The absence of CuO and Cu peaks in the XRD pattern indicated that the as-grown substrate was phase-pure cuprous oxide. SEM and XRD results thus indicated that the substrates synthesized by thermal oxidation were large-grain polycrystalline Cu_2O. Hall measurements indicated that the as-grown multicrystalline Cu_2O was p-type, with a hole concentration of 3.7×10^{13} cm^{-3} and a hole mobility of 65 cm^2 V^{-1} s^{-1} at room temperature, which are comparable to values reported in the literature for Cu_2O films prepared by an analogous method.[8,13]

B. Photoelectrochemical behavior under simulated AM 1.5 illumination

Fig. 2a displays the *J–E* behavior of Cu_2O photocathodes in contact with either CH_3CN–1.0 M $LiClO_4$–0.020 M $CoCp_2^+$–0.002 M $CoCp_2^0$ (red trace) or CH_3CN–1.0 M $LiClO_4$–0.020 M $Me_{10}CoCp_2^+$–0.002 M $Me_{10}CoCp_2^0$ (blue trace). In contact with the $CoCp_2^{+/0}$ redox couple, Cu_2O photocathodes typically exhibited V_{oc} values between 500 and 550 mV. In contrast, in contact with the $Me_{10}CoCp_2^{+/0}$ redox couple, Cu_2O photocathodes exhibited V_{oc} values between 780 and 820 mV. In both cases, the Cu_2O photocathodes exhibited J_{sc} values between 3 and 4 mA cm^{-2} and fill factors of 0.5–0.6.

In the dark and under forward bias, the stabilized electrodes passed only anodic current, as expected for a reversible photoelectrochemical system whose absolute anodic current was limited by the low concentration of the reduced species, either $CoCp_2^0$ or $Me_{10}CoCp_2^0$, respectively. In contrast to stabilized electrodes, freshly etched Cu_2O electrodes displayed V_{oc} values >1 V under 1 sun of illumination, and V_{oc} = 0.3–0.4 V in the dark. The potential offset however was only observed prior to the first scan of the electrode. After passing a few mC cm^{-2} of cathodic charge, the dark open-circuit voltage stabilized at 0.0 V, and the open-circuit voltage under 1 sun of illumination stabilized near 800 mV for Cu_2O/CH_3CN–$Me_{10}CoCp_2^{+/0}$ contacts and near 520 mV for Cu_2O/CH_3CN–$CoCp_2^{+/0}$ contacts during several hour time period over which the experimental data were collected.

C. Spectral response in photoelectrochemical cells

Fig. 2b shows the external quantum yield (Φ_{ext} or EQE, light blue triangles) and the estimated internal quantum yield (Φ_{int} or IQE, dark blue squares) of Cu_2O photocathodes in contact with CH_3CN–$Me_{10}CoCp_2^{+/0}$. The external quantum yield peaked at 0.8 near 500 nm, with significant losses in both the blue and red spectral regions. Reflection losses were estimated using the Fresnel equations with the refractive indices of glass, CH_3CN and Cu_2O in the spectral range of interest. The refractive index of the Cu_2O substrates was measured by spectroscopic ellipsometry (see ESI, Fig. S1†). The optical reflection in the cell contributed ~15 to 20% to the incident photon loss, across the entire spectral range. The internal quantum yield, corrected for solution optical absorption (see ESI, Fig. S2†) and reflection losses, showed near-unity carrier collection in the 400 to 500 nm spectral range. The effective collection length, L_{eff}, was determined to be 490 nm by fitting the spectral response data to eqn (1) (Fig. 2b inset):[32]

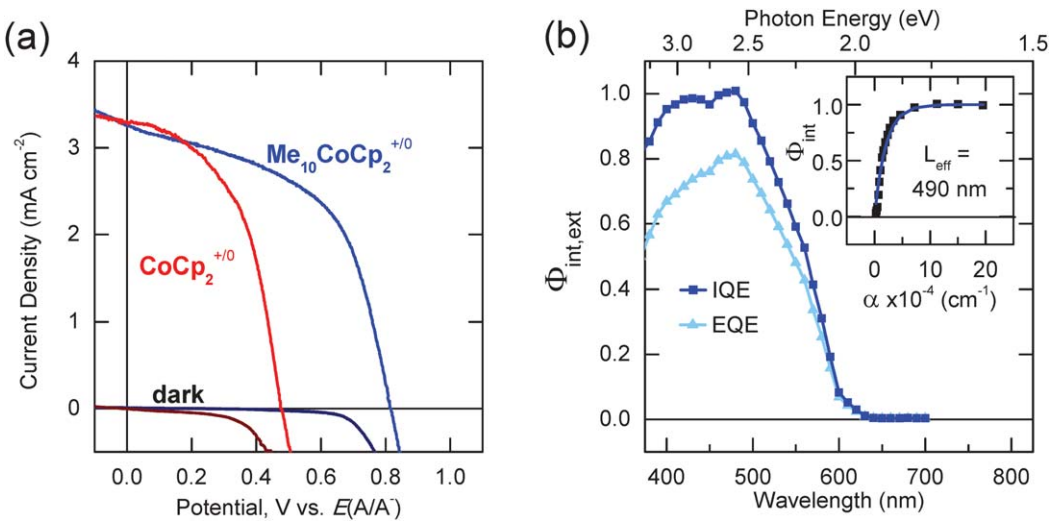

Fig. 2 (a) Current density–potential characteristics of Cu_2O photocathodes in the dark and under ELH-simulated 1 sun illumination in contact with CH_3CN–1.0 M $LiClO_4$ containing 0.020 M $Me_{10}CoCp_2^+$–0.002 M $Me_{10}CoCp_2$ (blue) or 0.020 M $CoCp_2^+$–0.002 M $CoCp_2$ (red), respectively. (b) Spectral response of Cu_2O photocathodes in CH_3CN–1.0 M $LiClO_4$–0.0020 M $Me_{10}CoCp_2^+$–0.0002 M $Me_{10}CoCp_2$, where the internal quantum yield is calculated from the external quantum yield using estimates of the solution optical absorption data and reflection losses.

$$\Phi(\lambda)_{\text{int}} = \frac{\int_0^{L_{\text{eff}}} q\Gamma_0\alpha(\lambda)e^{-\alpha(\lambda)x}dx}{q\Gamma_0} = 1 - e^{-\alpha(\lambda)L_{\text{eff}}} \quad (1)$$

where $q\Gamma_0\alpha(\lambda)e^{-\alpha(\lambda)x}$ is the electron–hole generation rate, Γ_0 is the incident photon flux per unit area, and $\alpha(\lambda)$ is the absorption coefficient of Cu_2O substrates at each wavelength (see ESI, Fig. S1†).

D. Light intensity dependence

Fig. 3a shows the effects of illumination intensity on the current density–voltage characteristics of Cu_2O/CH_3CN–$Me_{10}CoCp_2^{+/0}$ contacts. The maximum illumination intensity from the W–halogen ELH-type illumination corresponded to 100 mW cm^{-2}, *i.e.* 1 sun, whereas a series of neutral density filters was used to attenuate the light intensity to ~2.3 mW cm^{-2}. Fig. 3b shows the integrated external quantum yield as a function of the applied potential, where the integrated external quantum yield is the fraction of the observed photocurrent density relative to the estimated total photon flux at all energies above the Cu_2O band gap. The discrepancy between the absolute value of the integrated external quantum yield and the spectral response data shown in Fig. 2b is attributable to solution absorption. The integrated external quantum yield at J_{sc} increased as the light intensity decreased. The increase in Φ_{ext} is attributable to the decreased concentration of the highly absorbing $Me_{10}CoCp_2^0$ species that is generated near the electrode surface at low cathodic current densities.

The V_{oc} of a semiconductor/liquid junction is given by eqn (2), where n is the diode quality factor, k_B is the Boltzmann constant, T is the temperature (in Kelvin), q is the (unsigned) charge on an electron, J_{ph} is the photocurrent density, and J_0 is the exchange-current density:

$$V_{oc} = \frac{nk_BT}{q}\ln\left(\frac{J_{ph}}{J_0}\right) \quad (2)$$

For a photoconductor, when the series resistance of the photoelectrode is sufficiently large, the slope of the J–V behavior near V_{oc} is expected to be inversely proportional to the majority-carrier (hole) concentration (N_A) in the photoelectrode.[32] The hole concentration (N_A) for Cu_2O photoelectrodes as a function of light intensity was thus computed from the cell series resistance that was estimated by fitting the slope of the J–E data in the region of V_{oc}[32] (Fig. 3a inset). The deduced hole concentration showed a linear relationship on light intensity, consistent with other reports of photoconductivity in Cu_2O.[33,34] Consistently, at illumination intensities near 1 sun, a diode ideality factor of approximately 2.1 (Fig. 3b, inset) was obtained from the slope of V_{oc} *vs.* J_{sc} (eqn (2)). The error bars in the inset represent the standard deviation from four samples that were analyzed under a series of illumination intensities.

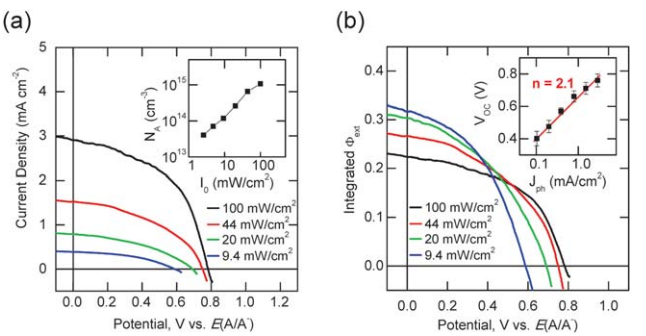

Fig. 3 (a) Current density–potential characteristics and (b) external quantum yield as a function of ELH illumination intensity for Cu_2O photocathodes in contact with CH_3CN–1.0 M $LiClO_4$ – 0.020 M $Me_{10}CoCp_2^+$–0.002 M $Me_{10}CoCp_2$. The external quantum yield was calculated using the theoretical maximum current density for the ELH illumination intensity. (b, inset) Linear fits to V_{oc} as a function of ELH illumination intensity using the ideal diode equation gave estimates of the diode ideality factor for the junction.

E. Stability of Cu_2O photoelectrodes

Fig. 4a displays J–E data for freshly etched Cu_2O electrodes in contact with the aqueous $MV^{2+/+}$ redox couple (purple), as well as the J–E behavior of $Cu_2O/Me_{10}CoCp_2^{+/0}$ contacts before (blue) and after (orange) photoelectrochemical measurements of $Cu_2O/MV^{2+/+}$ (aq) contacts. The J–E data of the $Cu_2O/MV^{2+/+}$ (aq) contacts exhibited V_{oc} < 200 mV. Moreover, after the

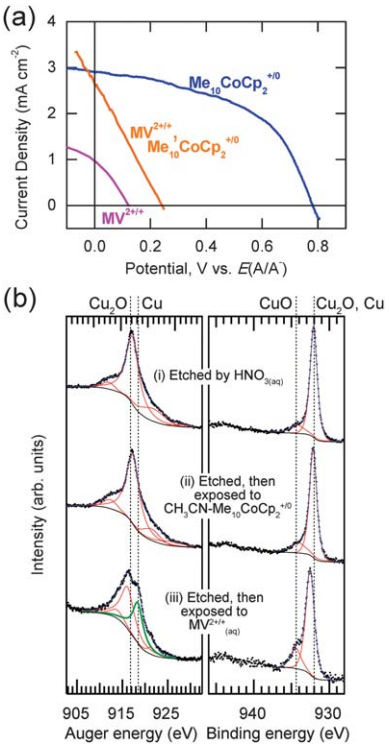

Fig. 4 (a) Current density–potential characteristics under ELH-simulated 1 sun illumination of freshly etched Cu_2O photocathodes in contact with CH_3CN–1.0 M $LiClO_4$–0.020 M $Me_{10}CoCp_2^+$–0.002 M $Me_{10}CoCp_2$ (blue); etched, exposed to H_2O–0.5 M K_2SO_4–0.050 M MV^{2+} (aq) and then in contact with CH_3CN–1.0 M $LiClO_4$–0.020 M $Me_{10}CoCp_2^+$–0.002 M $Me_{10}CoCp_2$ (orange); etched Cu_2O photocathodes in contact with H_2O–0.5 M K_2SO_4–0.050 M MV^{2+} (aq) (purple). (b) Cu LMM Auger spectra (left) and Cu($2p_{3/2}$) XP spectra (right) for chemically treated Cu_2O: (i) etched by aqueous HNO_3; (ii) etched then exposed to CH_3CN–$Me_{10}CoCp_2^{+/0}$; (iii) etched then exposed to H_2O–0.5 M K_2SO_4–0.050 M MV^{2+} (aq).

measurements, visible Cu precipitation was observed at the electrode surface, consistent with severe photocorrosion. Freshly etched Cu_2O electrodes demonstrated $V_{oc} \approx 800$ mV in contact with CH_3CN–$Me_{10}CoCp_2^{+/0}$ electrolytes, but electrodes that had first been exposed to $MV^{2+/+}$ (aq) electrochemical scans under illumination exhibited $V_{oc} < 300$ mV in contact with $Me_{10}CoCp_2^{+/0}$. The degradation of the photoelectrochemical performance that was caused by photocorrosion of Cu_2O in aqueous methyl viologen experiments was, however, reversed by re-etching the Cu_2O electrodes in HNO_3 (aq).

The photoelectron spectra in Fig. 4b further elucidate the chemical transformations at the surface of Cu_2O electrodes. In Cu($2p_{3/2}$) photoelectron spectra, metallic Cu^0 exhibits a peak centered at 932.6 eV, whereas Cu_2O shows a peak at 932.4 eV, and CuO shows a primary photoelectron peak at 933.6 eV as well as secondary shake-up peaks at 940–945 eV.[35] Hence, the Cu($2p_{3/2}$) spectral region unambiguously identifies the presence of CuO surface species, but cannot readily resolve the 0.2 eV difference between Cu_2O and metallic Cu^0 surface species. In contrast, metallic Cu^0 produces a peak centered at 918.5 eV in the Cu LMM Auger electron region, whereas Cu_2O exhibits a signal at 916.8 eV, and CuO shows a signal at 917.8 eV.[35–38] The peak shapes observed in the Cu LMM Auger region can thus discriminate between Cu_2O and metallic Cu^0 surface species

Fig. 4b depicts the spectra from the Cu LMM Auger electron region (left) as well as the Cu($2p_{3/2}$) photoelectron region (right) observed for Cu_2O substrates that were either freshly etched (i), used as photoelectrodes under illumination in contact with CH_3CN–$Me_{10}CoCp_2^{+/0}$ (ii), or used as photoelectrodes under illumination in contact with $MV^{2+/+}$ (aq) (iii). In all cases, spectra were fit with Gaussian–Lorentzian peaks above a Shirley background, with the red traces denoting individual fitted peaks, the blue traces denoting the sum of the individual peaks, and the black traces denoting the baseline of the fitted spectra. While all of the XP spectra were well fit with two peaks, additional peaks at both high and low-binding energy were needed to effectively fit the Auger spectra. These additional peaks have been observed previously in the Auger LMM spectra of copper oxides.[34] As a guide between spectra, and for comparison with literature results, a dashed line has been included in the Auger spectra at 916.8 eV, indicative of the Cu_2O species, and another dashed line has been included at 918.5 eV, indicative of metallic Cu^0. A dashed line is shown in the XP spectra at 934.4 eV, indicative of CuO species, and another dashed line has been included at 932.1 eV, indicative of either Cu_2O or metallic Cu^0.

As shown in part (i) of Fig. 4b, the Cu($2p_{3/2}$) spectral region of the freshly etched Cu_2O surface showed a large peak at 932.1 eV and a smaller feature centered at 934.3 eV, indicating that little CuO or surface hydroxide was present on the surface of the sample. Further, the Cu LMM Auger peak at 917.1 eV, and the absence of any significant feature at 918.5 eV, indicate that the thermal oxidation of Cu foil to Cu_2O, and subsequent etching with HNO_3(aq), produced a Cu_2O surface that was free of metallic Cu^0. The Auger spectrum in part (i) and all further Auger spectra show features attributed to an additional peak towards the lower binding energy at ~912.5 eV and a further peak towards the higher binding energy at ~921.0 eV. These peaks are attributed to other LMM Auger transitions not principally diagnostic of copper oxidation.[34–37] By comparison with part (i), part (ii) of Fig. 4b demonstrates that the surface composition was essentially unchanged after photoelectrochemical experiments in contact with CH_3CN–$Me_{10}CoCp_2^{+/0}$. This result is consistent with the expected stability of Cu_2O in nonaqueous photoelectrochemical cells.

In contrast, use of the Cu_2O in contact with $MV^{2+/+}$(aq) yielded significant changes in the XP and Auger spectra, as shown in Fig. 4b, part (iii). In particular, the strongest feature in the Cu LMM Auger spectrum shifted from 917.1 eV to 916.4 eV, and an additional feature appeared at 918.5 eV, denoted by the bold, green fitted trace, which is ascribable to metallic Cu^0. Although not strictly quantitative due to the paucity of sensitivity factors and other calibrations for Auger spectra of copper oxides, the ratio of the area of the green fitted peak at 918.5 eV to the area of the peak centered at 916.4 eV was 0.56. Assuming similar probabilities for Auger emission and capture of secondary electrons from Cu_2O and Cu^0, Fig. 4b part (iii) thus clearly indicates the presence of significant quantities of interfacial metallic Cu^0. Thus, the Auger spectrum of Fig. 4b part (iii) corroborates the results described above, in which interfacial metallic Cu^0 formed by aqueous photocorrosion processes significantly degraded the photoelectrochemical performance of the Cu_2O/CH_3CN–$Me_{10}CoCp_2^{+/0}$ contact.

IV. Discussion

A. Open-circuit voltage of p-Cu_2O/CH_3CN contacts

The behavior of the semiconductor/liquid contacts investigated herein, in which the redox system in the liquid was not photoexcited but only served to transport the charge across the interface and to determine the equilibrium barrier-height of the solid/liquid contact, arose from the photogeneration, transport, and recombination processes in the p-Cu_2O, along with the space-charge field in the p-Cu_2O produced by charge equilibration between the Fermi levels of the Cu_2O and the redox species in the electrolyte. The resulting energy-conversion properties of such systems are thus directly analogous to those displayed by p-Cu_2O-based heterojunctions or homojunctions. The 820 mV open-circuit voltage of Cu_2O/CH_3CN–$Me_{10}CoCp_2^{+/0}$ contacts is significantly higher than the reported V_{oc} values of 595 mV[13] and 300 mV[14,15] for Cu_2O/ZnO, 400 mV for Cu_2O/CdO[12,16] and Cu_2O/Al-doped ZnO,[39] 270 mV for Cu_2O/ITO,[40] 240 mV for Cu_2O/Cu_xS,[41] or <430 mV for p–n-Cu_2O junctions,[42,43] and <400 mV for previous Cu_2O/liquid junctions.[22,44] The open-circuit voltages of photoelectrodes measured in a potentiostatic, three-electrode configuration are identical to those of full, regenerative, two-electrode, photoelectrochemical cells measured for the same solid/liquid contacts under the same injection levels.[30,45] These open-circuit voltages, representing the maximum free energy produced and available to be driven through an external load at steady state under the specified illumination conditions, and also are directly related to the open-circuit voltage, and thus maximum free energy produced, of a solid-state photovoltaic energy conversion device under the same illumination conditions.[30,45] The 3.2 eV electron affinity of cuprous oxide constrains the choices of redox couples appropriate for semiconductor/liquid junctions, because a very negative reduction potential is required to minimize the discontinuity

between the Cu_2O conduction-band edge and the solution reduction potential. For instance, the $CoCp_2^{+/0}$ formal reduction potential of −0.91 V *vs.* SCE[46] and the $Me_{10}CoCp_2^{+/0}$ formal reduction potential of −1.47 V *vs.* SCE[46] are close to the potential of the Cu_2O conduction-band edge of −1.6 V[26] *vs.* SCE. The difference between the V_{oc} values in Cu_2O/CH_3CN–$Me_{10}CoCp_2^{+/0}$ contacts and Cu_2O/CH_3CN–$CoCp_2^{+/0}$ contacts is thus related, as expected, to the different Nernstian potentials of the two redox couples, with the solution having the more negative Nernstian redox potential producing a higher barrier height, and thus a higher open-circuit voltage, than solutions having more positive Nernstian potentials.[45]

The observed open-circuit voltage is nonetheless lower than the V_{oc} expected from the bulk recombination limit for Cu_2O. The maximum theoretical V_{oc} of a semiconductor junction is determined by the bulk electronic properties of the semiconductor (eqn (3)):[29,32,47]

$$V_{oc} \cong \frac{kT}{q} \ln\left(\frac{J_{ph} L_n N_A}{q D_n n_i^2}\right) \quad (3)$$

where L_n is the minority-carrier (electron) diffusion length, N_A is the concentration of acceptors, n_i is the intrinsic carrier density, D_n is the minority-carrier diffusion coefficient (estimated by using $D_n = (\frac{m_h}{m_e}\mu_h)\frac{kT}{q}$, where μ_h is the hole mobility, and $\frac{m_h}{m_e} \approx 0.58$ is the effective mass ratio between the hole and the electron).[48–50] Using $N_A = 3.7 \times 10^{13}$ cm^{-3}, $D_n = 2.2$ cm^2 s^{-1}, $n_i = 2 \times 10^2$ cm^{-3}, and estimating L_n to be 100 nm to 10 μm, yields a value of 1.20–1.32 V as the maximum theoretical V_{oc} for Cu_2O photocathodes. Achieving the maximum theoretical V_{oc} will require the use of the redox couple with a more negative potential and the passivation of Cu_2O surface states.

B. Short-circuit current density of Cu_2O/CH_3CN contacts

The low observed J_{sc} values for Cu_2O photocathodes in contact with CH_3CN–$Me_{10}CoCp_2^{+/0}$ solutions can be quantitatively attributed to incomplete collection due to bulk recombination in the semiconductor and to incomplete absorption due to solution optical absorption and reflection losses. Table 1 shows the estimated J_{sc} values expected for Cu_2O photocathodes under AM 1.5 illumination, under ELH-simulated 1.0 sun of illumination, and under attenuated ELH-simulated 0.09 sun of illumination, given the various expected loss mechanisms. J_{sc}^{MAX} represents the theoretical maximum photocurrent density given the photon flux of the incident light that is above the 2.0 eV band gap of Cu_2O, using standard spectral data. J_{sc}^{IQE} refers to the expected photocurrent density, given the spectrum of the incident light and the energy dependence of the internal quantum yield. J_{sc}^{PEC} refers to the expected photocurrent density given the measured solution absorption and estimated reflection losses inherent in the photoelectrochemical cell in addition to internal collection losses. At ELH-simulated 1.0 sun illumination, the value J_{sc}^{EXP} is expected to be even less than J_{sc}^{PEC}, due to additional solution absorption caused by the $Me_{10}CoCp_2^0$ that is generated at the electrode surface under short-circuit conditions. However, at the attenuated ELH-simulated 0.09 sun illumination, the values of J_{sc}^{PEC} and J_{sc}^{EXP} are in agreement, because the photogenerated $Me_{10}CoCp_2^0$ is produced at a lower rate and can be removed effectively by convection. Routes to improving the photocurrent of the Cu_2O photocathodes in contact with a nonaqueous $Me_{10}CoCp_2^{+/0}$ solution include producing material with longer diffusion lengths and better red response, as well as utilizing a thin-layer photoelectrochemical cell[30] with minimized solution absorption.

Table 1 Analysis of photocurrent density for Cu_2O photocathodes, where J_{sc}^{MAX} corresponds to the theoretical maximum photocurrent density given the 2.0 eV band gap of Cu_2O and the spectrum of the incident light; J_{sc}^{IQE} corresponds to the expected photocurrent density given the reduced red response due to internal collection losses; J_{sc}^{PEC} corresponds to the expected photocurrent density given the estimated internal quantum yield, solution absorption and reflection losses; and J_{sc}^{EXP} is the observed photocurrent density under ELH illumination

Light source	J_{sc}^{MAX}/ mA cm^{-2}	J_{sc}^{IQE}/ mA cm^{-2}	J_{sc}^{PEC}/ mA cm^{-2}	J_{sc}^{EXP}/ mA cm^{-2}
AM 1.5	14.07	9.01	4.96	n/a
ELH	13.78	7.20	4.67	3.31
Attenuated ELH	1.30	0.68	0.44	0.41

V. Conclusions

Phase-pure, multicrystalline Cu_2O substrates were produced by thermal oxidation of Cu foils. P-type Cu_2O photoelectrodes were demonstrated to be stable and free of deleterious interfacial reactions in nonaqueous regenerative photoelectrochemical cells. Highly rectifying contacts were made to p-type Cu_2O using redox couples with very negative Nernstian potentials. In contact with CH_3CN–$Me_{10}CoCp_2^{+/0}$, Cu_2O photoelectrodes exhibited 820 mV open-circuit voltage, and near-unity internal quantum yield in the 400–500 nm spectral range. The observed short-circuit current density agreed well with the value expected after correction for solution optical absorption and reflection losses. The observation of high open-circuit voltages in the p-Cu_2O/liquid junction demonstrates that high efficiency p-Cu_2O solar energy conversion devices can be obtained provided that suitable emitter materials, that form high barrier-heights to Cu_2O substrates and that allow for rigorous control of the surface chemistry and surface passivation of p-Cu_2O absorbers, can be identified.

Acknowledgements

This work was supported by the Office of Energy Efficiency and Renewable Energy, US Department of Energy under Grant DE-FG36-08GO18006, the Caltech Center for Sustainable Energy Research (CCSER), and the Dow Chemical Company. One of us (GMK) acknowledges support under an NDSEG graduate fellowship.

References

1 C. Wadia, A. P. Alivisatos and D. M. Kammen, *Environ. Sci. Technol.*, 2009, **43**, 2072.
2 L. C. Olsen, F. W. Addis and W. Miller, *Sol. Cells*, 1982, **7**, 247.
3 B. P. Rai, *Sol. Cells*, 1988, **25**, 265.
4 J. A. Assimos and D. Trivich, *J. Appl. Phys.*, 1973, **44**, 1687.
5 F. L. Weichman, *Phys. Rev.*, 1960, **117**, 998.
6 A. A. Berezin and F. L. Weichman, *Solid State Commun.*, 1981, **37**, 157.

7 D. Trivich, E. Y. Wang, R. J. Komp, K. Weng and A. Kakar, *J. Electrochem. Soc.*, 1977, **124**, C318.
8 A. O. Musa, T. Akomolafe and M. J. Carter, *Sol. Energy Mater. Sol. Cells*, 1998, **51**, 305.
9 L. C. Olsen, R. C. Bohara and M. W. Urie, *Appl. Phys. Lett.*, 1979, **34**, 47.
10 J. Herion, E. A. Niekisch and G. Scharl, *In the 14th IEEE Photovoltaic Specialists Conference*, 1980.
11 E. Y. Wang, D. Trivich, R. J. Komp, T. F. Huang and D. J. Brinker, *In the 14th IEEE Photovoltaic Specialists Conference*, 1980, p. 458.
12 L. Papadimitriou, N. A. Economou and D. Trivich, *Sol. Cells*, 1981, **3**, 73.
13 A. Mittiga, E. Salza, F. Sarto, M. Tucci and R. Vasanthi, *Appl. Phys. Lett.*, 2006, **88**, 163502.
14 K. Akimoto, S. Ishizuka, M. Yanagita, Y. Nawa, G. K. Paul and T. Sakurai, *Sol. Energy*, 2006, **80**, 715.
15 J. Herion, E. A. Niekisch and G. Scharl, *Sol. Energy Mater.*, 1980, **4**, 101.
16 Y. Hames and S. E. San, *Sol. Energy*, 2004, **77**, 291.
17 S. W. Boettcher, J. M. Spurgeon, M. C. Putnam, E. L. Warren, D. B. Turner-Evans, M. D. Kelzenberg, J. R. Maiolo, H. A. Atwater and N. S. Lewis, *Science*, 2010, **327**, 185.
18 J. R. Maiolo, H. A. Atwater and N. S. Lewis, *J. Phys. Chem. C*, 2008, **112**, 6194.
19 J. R. Maiolo, B. M. Kayes, M. A. Filler, M. C. Putnam, M. D. Kelzenberg, H. A. Atwater and N. S. Lewis, *J. Am. Chem. Soc.*, 2007, **129**, 12346.
20 M. J. Price and S. Maldonado, *J. Phys. Chem. C*, 2009, **113**, 11988.
21 M. J. N. Pourbaix, *Thermodynamics of Dilute Aqueous Solutions*, 1949.
22 G. Nagasubramanian, A. S. Gioda and A. J. Bard, *J. Electrochem. Soc.*, 1981, **128**, 2158.
23 G. Vanamerongen, D. Guyomard and M. Herlem, *Sol. Energy Mater.*, 1981, **4**, 435.
24 J. L. Sculfort, D. Guyomard and M. Herlem, *Electrochim. Acta*, 1984, **29**, 459.
25 Y. Tachibana, R. Muramoto, H. Matsumoto and S. Kuwabata, *Res. Chem. Intermed.*, 2006, **32**, 575.
26 J. A. Assimos and D. Trivich, *Phys. Status Solidi A*, 1974, **26**, 477.
27 L. M. Wong, S. Y. Chiam, J. Q. Huang, S. J. Wang, J. S. Pan and W. K. Chim, *J. Appl. Phys.*, 2010, **108**, 033702.
28 M. Okeeffe and W. J. Moore, *J. Chem. Phys.*, 1962, **36**, 3009.
29 N. S. Lewis, *J. Electrochem. Soc.*, 1984, **131**, 2496.
30 J. F. Gibbons, G. W. Cogan, C. M. Gronet and N. S. Lewis, *Appl. Phys. Lett.*, 1984, **45**, 1095.
31 A. J. Bard and L. R. Faulkner, *Electrochemical Methods, Fundamentals and Applications*, Wiley, 2nd edn, 2000.
32 S. M. Sze, *Physics of Semiconductor Devices*, John Wiley and Sons, New York, 3rd edn, 1981.
33 E. Fortin, M. Zouaghi and J. P. Zielinge, *Phys. Lett. A*, 1967, **24**, 180.
34 J. Spyridel., J. Stoimeno. and N. Economou, *Phys. Status Solidi B*, 1967, **20**, 623.
35 S. Poulston, P. M. Parlett, P. Stone and M. Bowker, *Surf. Interface Anal.*, 1996, **24**, 811.
36 J. P. Tobin, W. Hirschwald and J. Cunningham, *Appl. Surf. Sci.*, 1983, **16**, 441.
37 T. H. Fleisch and G. J. Mains, *Appl. Surf. Sci.*, 1982, **10**, 51.
38 G. Panzner, B. Egert and H. P. Schmidt, *Surf. Sci.*, 1985, **151**, 400.
39 T. Minami, H. Tanaka, T. Shimakawa, T. Miyata and H. Sato, *Jpn. J. Appl. Phys.*, 2004, **43**, L917.
40 W. M. Sears, E. Fortin and J. B. Webb, *Thin Solid Films*, 1983, **103**, 303.
41 R. P. Wijesundara, L. D. R. D. Perera, K. D. Jayasuriya, W. Siripala, K. T. L. De Silva, A. P. Samantilleke and I. M. Dharmadasa, *Sol. Energy Mater. Sol. Cells*, 2000, **61**, 277.
42 C. M. McShane, W. P. Siripala and K. S. Choi, *J. Phys. Chem. Lett.*, 2010, **18**, 2666.
43 K. H. Han and M. Tao, *Sol. Energy Mater. Sol. Cells*, 2009, **93**, 153.
44 T. Mahalingam, J. S. P. Chitra, J. P. Chu, H. Moon, H. J. Kwon and Y. D. Kim, *J. Mater. Sci.: Mater. Electron.*, 2006, **17**, 519.
45 M. X. Tan, P. E. Laibinis, S. T. Nguyen, J. M. Kesselman, C. E. Stanton and N. S. Lewis, *Prog. Inorg. Chem.*, 1994, **41**, 21.
46 J. L. Robbins, N. Edelstein, B. Spencer and J. C. Smart, *J. Am. Chem. Soc.*, 1982, **104**, 1882.
47 H. J. Hovel, *Semiconductors and Semimetals*, Academic, New York, 1975, vol. 11.
48 J. W. Hodby, T. E. Jenkins, C. Schwab, H. Tamura and D. Trivich, *J. Phys. C: Solid State Phys.*, 1976, **9**, 1429.
49 A. Goltzene and C. Schwab, *Phys. Status Solidi B*, 1979, **92**, 483.
50 G. Dasbach, D. Frohlich, H. Stolz, R. Klieber, D. Suter and M. Bayer, *Fourth International Conference on Physics of Light-Matter Coupling in Nanostructures (PLMCN4)* 2005, 2, 886.

